Journal of Sound and Vibration (1997) **207**(3), 403–418

MULTI-MODE ANALYSIS OF BEAM-LIKE STRUCTURES SUBJECTED TO DISPLACEMENT-DEPENDENT DRY FRICTION DAMPING

W. W. WHITEMAN

Department of Civil and Mechanical Engineering, United States Military Academy, West Point, NY 10996, *U.S.A.*

AND

A. A. FERRI

School of Mechanical Engineering, Georgia Institute of Technology, Atlanta, GA 30332-0405, *U.S.A.*

(*Received* 16 *June* 1995, *and in final form* 9 *May* 1997)

A multi-mode analysis of a beam-like structure undergoing transverse vibration and subjected to a displacement-dependent friction force is conducted. The system model uses a ramp configuration to increase the normal force of the dry friction damper proportional to the beam's transverse displacement. The system is studied by using harmonic balance as an approximate analytical solution and then by using a time integration method. Interesting findings include the appearance of internal resonance peaks when multiple beam modes are considered. Also, as with the earlier single-degree-of-freedom study, two dynamic response solutions exist at certain parameter values. It is found that the ability to control the amplitude of the response is a function of the frequency range considered. In general, near modal resonance peaks, the amplitude of the response decreases with increasing ramp angle. However, in an "overlapping" region between resonance peaks, the amplitude of the response actually increases with increasing ramp angle. It is also found that the damping contribution from the displacement-dependent dry friction damper is "linear structural-like" in nature and relatively insensitive to the amplitude of the response. This result suggests that in the case of turbine or compressor blades, this type of damping arrangement may be effective in the suppression of flutter.

© 1997 Academic Press Limited

1. INTRODUCTION

This paper considers the dynamic behavior of beam-like structures undergoing transverse vibration and damped by displacement-dependent dry friction forces. Most studies assume dry friction forces to be proportional to a constant normal force acting across the sliding interface. Several studies, however, have explored the case where friction forces are dependent on the slip displacement across the frictional interface [1–12]. While displacement-dependence can always be expected in real systems, its effects on dynamic behavior are not fully understood.

To include displacement-dependency, the normal force is allowed to vary with transverse displacement as a result of the geometry of an attached dry friction damper. As seen in Figure 1, this effect is modelled with a passive configuration using a ramp function to increase the normal force linearly with displacement. Perhaps the most direct application of this system is in the study of a turbomachinery blade with a shroud interface. Other applications might include aerospace as well as civil engineering structures.

0022–460X/97/430403 + 16 $25.00/0/sv971140 © 1997 Academic Press Limited

This study also includes multi-degree-of-freedom (MDOF) modelling. While a single-degree-of-freedom (SDOF) model is sometimes a good approximation, or one mode projection of more physically realistic MDOF systems, multi-mode models are often necessary to predict the dynamics of complex systems accurately and to describe their behavior over a wide frequency range more fully. The MDOF model included in this paper is particularly desirable for turbine blade applications in which the natural frequencies and mode shapes depend on whether or not the friction interface of the blade is undergoing slip or is fully stuck. Multiple DOFs are needed for one model to accommodate all the possible types of responses [13]. Furthermore, the modes of response can change over the frequency range studied. As the frequency of excitation is varied, the structure may evolve from having a locked-up interface to having a slipping interface, and the behavior may change dramatically. It should be emphasized with the MDOF model that the structure may undergo motion even though the interface is fully locked up. In this case, the interface behaves like a pinned connection along the span. Multi-mode solutions of dry friction damped systems have been considered by several authors. Most relevant to the present study is the work of Ferri and Dowell [14, 15] in which beam structures with attached dry friction dampers were examined. Other references are cited in reference [16].

This paper is a direct extension of an earlier study by Whiteman and Ferri [17] which was a SDOF analysis of the same beam-like model depicted in Figure 1. Comparisons are made between the results of this past single-mode and present multi-mode analysis. The present paper includes proportional modal damping which was not included in the earlier SDOF study. Results from this paper confirm that a system with displacement-dependent friction forces can exhibit significantly different behavior than systems with constant friction forces. In fact, a key finding from the earlier work and this study is that the damping contribution from dry friction alone is "linear structural-like" in nature and relatively insensitive to the amplitude of the response. This result suggests that in the case of turbine or compressor blades, a displacement-dependent damping arrangement may be effective in the suppression of flutter.

Development of the model and governing equations of motion are presented in the following section. Component mode synthesis is carried out by using the constraint condition and a Lagrange multiplier approach to allow a multi-mode analysis to be performed. The resulting system of equations is highly non-linear and an analytical investigation in which the dry friction non-linearities are approximated by their first

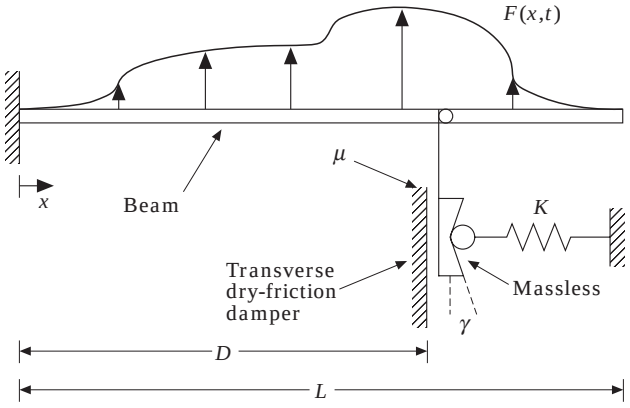

Figure 1. System model: transverse frictional interface, normal force proportional to beam transverse displacement.

TABLE 1

Parameter values

Item	Symbol	Value
Mass/unit length (kg/m)	$m(x)$	0·6361
Beam length (m)	L	0·3
Friction damper location (m)	D	0·2
Young's Modulus (N/m^2)	E	$7{\cdot}3 \times 10^{10}$
Moment of Inertia (m^4)	I	$1{\cdot}325 \times 10^{-10}$
Forcing amplitude (N)	F	10·0
Forcing location (m)	x_F	0·3
Spring stiffness (N/m)	K	100 000
Coefficient of friction	μ	0·5
Modal damping ratios	$\zeta_1, \zeta_2, \ldots, \zeta_{NM}$	0·01
Preload force (N)	N_0	5

harmonic is presented in section 3. Section 4 presents an "exact" solution by way of a Runge–Kutta time integration scheme. Results from the harmonic balance analysis are then compared to the "exact" solution in section 5. Section 6 is a detailed analysis of the damping characteristics of the system. Conclusions are presented in Section 7.

2. DEVELOPMENT OF THE MODEL AND GOVERNING EQUATIONS

Figure 1 shows the model to be studied. Table 1 lists the baseline parameter values. These beam parameters were chosen to approximate an actual turbomachinery fan blade; however the emphasis is on qualitative trends in the dynamic behavior of generic beam-like structures.

The beam flexural displacement $w(x, t)$ can be approximated using NM assumed modes:

$$w(x, t) = \sum_{i=1}^{NM} z_i(t)\phi_i(x), \tag{1}$$

where x is the spatial coordinate measured from the clamped end of the beam, t is time, $z_i(t)$ is the modal amplitude of the ith assumed mode for the beam in flexure, $\phi_i(x)$. The assumed modes are taken to be the exact fixed–free eigenmodes of a uniform clamped–free beam:

$$\phi_i(x) = \frac{1}{\sqrt{mL}}\left\{\cosh\frac{\lambda_i x}{L} - \cos\frac{\lambda_i x}{L} - \left(\frac{\cosh\lambda_i + \cos\lambda_i}{\sinh\lambda_i + \sin\lambda_i}\right)\left(\sinh\frac{\lambda_i x}{L} - \sin\frac{\lambda_i x}{L}\right)\right\}, \tag{2}$$

where λ_i is the ith root of the characteristic equation

$$\cosh\lambda_i \cos\lambda_i + 1 = 0.$$

The method of component mode synthesis [18] is used to develop the governing equations. As such, the system is disassembled into two parts [15]. The first part is a linear, cantilever beam of length L, mass per unit length $m(x)$, flexural rigidity $EI(x)$, and viscous modal damping. The second part is a massless, displacement-dependent non-linear dry friction damper. Treating these subsystems separately, the kinetic energy of the beam is

$$T = \frac{1}{2} \sum_{i=1}^{NM} m_i \dot{z}_i^2, \tag{3}$$

where m_i is the modal mass of the ith beam mode:

$$m_i = \int_0^L m(x) \phi_i^2 (x) \, \mathrm{d}x.$$

It can be shown that the eigenfunctions $\phi_i (x)$ as given in equation (2) have been normalized such that all modal masses are unity.

The potential energy of the beam is

$$V = \frac{1}{2} \sum_{i=1}^{NM} m_i \omega_i^2 z_i^2, \tag{4}$$

where the modal stiffness of the ith beam mode is given by

$$m_i \omega_i^2 = \int_0^L EI(x) \phi_i'' (x)^2 \, \mathrm{d}x.$$

The virtual work on the beam due to a point force $F(t)$ applied at the end of the beam and viscous modal damping is

$$\delta W_B = \sum_{i=1}^{NM} (F(t) \phi_i (L) - 2\zeta_i \omega_i \dot{z}_i) \, \delta z_i, \tag{5}$$

where ζ_i are the beam modal damping ratios and ω_i are the natural frequencies of the assumed beam modes.

The kinetic and potential energies of the dry friction damper are assumed to be zero. The virtual work of the damper consists of two parts. One part is associated with the Coulombic force, μN_x, where μ is the sliding coefficient of friction (assumed to be equal to the static coefficient of friction) and N_x is the normal force perpendicular to the sliding interface. The second part accounts for the tangential component or in-plane restoring force, N_y, between the roller and the ramp surface:

$$\delta W_D = -\mu N_x \operatorname{sgn} (\dot{w}_d) \, \delta w_d - N_y \, \delta w_d, \tag{6}$$

where w_d is the displacement of the damper and

$$N_x = N_0 + K \tan \gamma |w_d|, \qquad N_y = (N_0 + K \tan \gamma |w_d|) \tan \gamma \operatorname{sgn} (\mathrm{w_d}).$$

Note that the transverse force N_x is composed of two parts. The first part, N_0, is the preload present in the spring K. The second part grows linearly with the damper displacement due to the ramp angle, γ.

A constraint, g, is introduced that states that the dry friction damper and the beam must remain in contact at all times; i.e., the beam displacement at the point of attachment, $x = D$, must remain equal to w_d at all times:

$$g(z_1, z_2, \ldots, z_{NM}, w_d) = w(D, t) - w_d = \sum_{i=1}^{NM} z_i \, \phi_i (D) - w_d = 0. \tag{7}$$

The "modified Lagrangian" used in the component mode synthesis technique [18] is

$$L^* = T - V + \beta g, \tag{8}$$

where β is the Lagrange multiplier (force of constrant). Lagrange's equations may now be applied:

$$\mathrm{d}/\mathrm{d}t(\partial L^*/\partial \dot{q}_i) - \partial L^*/\partial q_i = Q_i, \qquad i = 1, NM + 1, \tag{9}$$

where the generalized co-ordinates q_i are z_i for $i = 1$, NM and $q_{NM+1} = w_d$. Q_i are the generalized forces that are obtained from the respective virtual work terms. The resulting equations are

$$m_i [\ddot{z}_i + 2\zeta_i \omega_i \dot{z}_i + \omega_i^2 z_i] = F(t)\phi_i (L) + \beta(t)\phi_i (D), \qquad i = 1, NM, \tag{10}$$

$$\mu(N_0 + K \tan \gamma |w_d|)\mathrm{sgn}\,(\dot{w}_d) + (N_0 + K \tan \gamma |w_d|) \tan \gamma \ \mathrm{sgn}\,(w_d) + \beta(t) = 0. \tag{11}$$

These plus the constraint (7) form a system of $NM + 2$ equations in as many unknowns (z_i, w_d, β). One may note that with only one non-linear damper, component mode synthesis has produced a system of governing equations consisting of $NM + 1$ linear equations, and a *single non-linear equation*.

3. HARMONIC BALANCE ANALYSIS

Considering the case of a harmonic forcing function, $F(t) = F \cos(\omega t)$, the harmonic balance method can be applied to approximate the response of the beam. In this study, the assumption will be made that a single harmonic adequately represents the response of the system to harmonic excitation. Termed first order harmonic balance, this assumption is valid provided that the displacement at the frictional interface is relatively free of sticking.

Although this study will consider only first order harmonic balance, it is instructive to discuss some of the features of multi-harmonic analyses. Several authors have considered the inclusion of higher harmonics in the analysis of dry friction damped systems [14, 19–22]. As discussed in reference [14], as more harmonics are included, the displacements, strains, and even the friction force is shown to converge to results obtained using time integration. Note that the harmonic balance method can only determine the steady state response of a system, which can be stable or unstable. Depending on the system and excitation parameters, the harmonic balance method may yield zero, one, or many solutions. Usually, the period of the response is chosen to coincide with that of the excitation; however, a subharmonic response could be easily accomodated by expanding the response in terms of integer multiples of the subharmonic response of interest [22]. Finally, the numerical efficiency of harmonic balance methods can be considered. Since the harmonic balance method yields the steady state solution directly, there is no need to solve first for a transient response. This is especially helpful in the case of lightly damped systems with widely spaced resonant frequencies in which case time integration methods are burdened by long duration transients and small time steps. As shown below, first order harmonic balance requires the solution of a system of linear algebraic equations plus a *single quadratic equation*; thus its computational demands are extremely modest. However, as more harmonics are included, the number and complexity of the system of non-linear algebraic equations grows. This suggests that at some critical number of harmonics, it would be more efficient to obtain the steady state response through numerical integration.

Retaining only the fundamental harmonic, one may express the forcing function and unknowns, z_i, β, w_d, as

$$F(t) = F^c \cos(\omega t) + F^s \sin(\omega t), \qquad z_i = z_i^c \cos(\omega t) + z_i^s \sin(\omega t), \qquad \text{for } i = 1, NM, \tag{12, 13}$$

$$\beta(t) = \beta^c \cos(\omega t) + \beta^s \sin(\omega t), \qquad w_d = w_d^c \cos(\omega t) + w_d^s \sin(\omega t) = W_d \cos(\omega t + \theta). \tag{14}$$

Since only one damper is present, one can simplify the analysis without loss of generality by specifying the phase of the damper response such that $\theta = 0$:

$$w_d = w_d^c \cos(\omega t). \tag{15}$$

Substituting equations (12) through (15) into equations (7), (10) and (11) and balancing harmonics yields

$$m_i [(-\omega^2 + \omega_i^2) z_i^c + 2\zeta_i \omega \omega_i z_i^s] = F^c \phi_i(L) + \beta^c \phi_i(D), \qquad \text{for } i = 1, NM, \tag{16}$$

$$m_i [(-\omega^2 + \omega_i^2) z_i^s - 2\zeta_i \omega \omega_i z_i^c] = F^s \phi_i(L) + \beta^s \phi_i(D), \qquad \text{for } i = 1, NM, \tag{17}$$

$$\beta^s - (2/\pi)\mu(K \tan \gamma w_d^c + 2N_0) = 0, \qquad \beta^c + \tan \gamma (K \tan \gamma w_d^c + (4/\pi)N_0) = 0, \tag{18, 19}$$

$$\sum_{i=1}^{NM} z_i^c \phi_i(D) - w_d^c = 0, \qquad \sum_{i=1}^{NM} z_i^s \phi_i(D) = 0, \tag{20, 21}$$

where the following fundamental harmonic approximations have been used:

$$\operatorname{sgn}(w_d^c \cos(\omega t)) \approx (4/\pi)\cos(\omega t), \qquad \operatorname{sgn}(-\omega w_d^c \sin(\omega t)) \approx -(4/\pi)\sin(\omega t), \tag{22, 23}$$

$$|\cos(\omega t)| \operatorname{sgn}(-\omega w_d^c \cos(\omega t)) = \cos(\omega t),$$

$$|\cos(\omega t)| \operatorname{sgn}(-\omega w_d^c \sin(\omega t)) \approx -(2/\pi)\sin(\omega t). \tag{24, 25}$$

Equations (16) through (21) are a set of $2NM + 4$ linear algebraic equations and may be solved as follows. Solve equations (16) and (17) for z_i^c and z_i^s in terms of F^c, F^s, β^c and β^s. Solve equations (18) and (19) for β^c and β^s in terms of w_d^c. Substituting the expressions obtained for z_i^c, z_i^s, β^c and β^s into equations (20) and (21) yields two equations for w_d^c, F^c and F^s. Noting that the amplitude of the harmonic forcing function, $F(t)$, satisfies the relation $F^2 = (F^c)^2 + (F^s)^2$, one may obtain a single quadratic relation for the displacement at the damper, w_d^c. Once w_d^c is solved for, F^c and F^s can be determined from equations (20) and (21), and the force of constraint, β, can be found from equations (18) and (19). Finally, the modal amplitudes can be found from equations (16) and (17), and one may calculate the displacement, velocity, and accelerations anywhere along the length of the beam.

Prior to plotting results, a non-dimensionalization scheme is used to scale the results. This scheme will be similar to that used in the earlier work on this system by Whiteman and Ferri [17] for comparison purposes. Recall from equation (1) that $w(x, t)$ is the actual beam flexural displacement, $z_i(t)$ are the modal amplitudes, and $\phi_i(x)$ are the mass-normalized shape functions or assumed beam bending modes using fixed–free boundary conditions (2). The modal amplitudes are non-dimensionalized such that

$$\tilde{z}_i(t) = m_1 \omega_1^2 z_i(t)/F, \tag{26}$$

where F is the amplitude of the harmonic force applied to the beam at $x = L$, $F(t) = F \cos \omega t$. A non-dimensional frequency ratio is also introduced as

$$r = \omega/\omega_1. \tag{27}$$

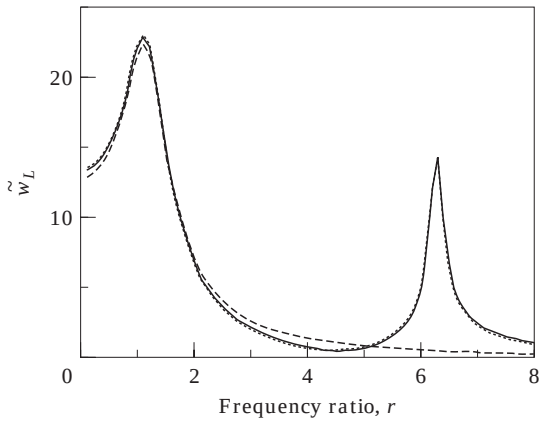

Figure 2. Harmonic balance results in terms of frequency response: ramp angle = 5°; - - - -, $NM = 1$; ——, $NM = 2$; ····, $NM = 5$.

The non-dimensional beam displacement is defined as

$$\tilde{w}(x, t) = \sum_{i=1}^{NM} \tilde{z}_i(t)\phi_i(x). \tag{28}$$

For fixed force amplitudes, one may now plot frequency response curves obtained using harmonic balance. Figure 2 is a plot of the harmonic balance prediction for the non-dimensional beam end displacement, $\tilde{w}_L$, for the parameter values given in Table 1 for a ramp angle of 5° and a varying number of assumed modes. Attention is restricted to a range of excitation frequencies containing the first two system resonances. It is evident from this plot that the harmonic balance results converge with the inclusion of only two modes in this frequency range of interest.

Figure 3 is a similar plot for a ramp angle of 35°. It is interesting to note that now three modes are required for convergence. This occurs as a result of the damper constraint becoming stiffer, necessitating the inclusion of higher modes of vibration.

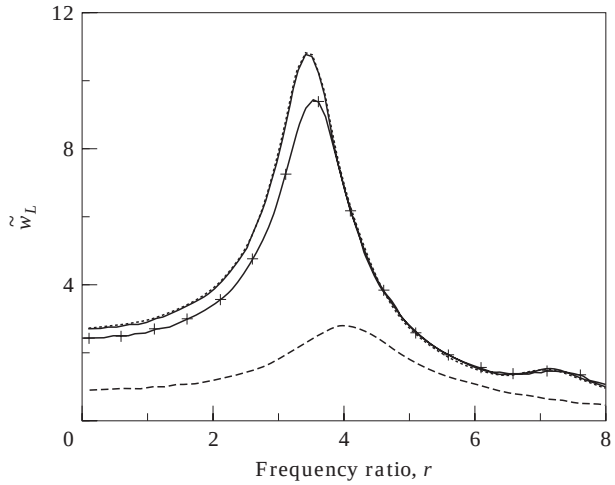

Figure 3. Harmonic balance results: ramp angle = 35°, NM Values: - - - -, 1; + +, 2; ——, 3; ····, 5.

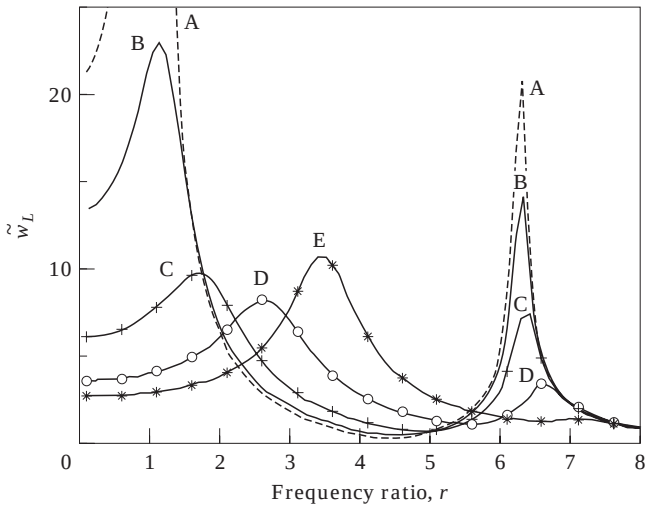

Figure 4. Harmonic balance results: $NM = 3$, ramp angles (°) = 0: - - - -, 0 (A); ——, 5 (B); + + +, 14 (C); —○—, 25 (D); —∗—, 35 (E).

Using three assumed modes, Figure 4 gives harmonic balance results for various ramp angles, γ. From a design standpoint, the implications of this plot are significant in determining how to control the magnitude of the response using passive friction damping. It is seen that the damper's effectiveness depends strongly on the ramp angle and the frequency range in which one is operating. For low frequency ratios, $r < 1{\cdot}8$, and for frequency ratios above 5·5, the magnitude of the response becomes increasingly smaller as the ramp angle is increased. In the mid-frequency range of $3 < r < 5$, however, the magnitude of the response increases for larger ramp angles. This "overlapping" of the response curves was also noted in the earlier SDOF study of this system [17], but has a *much more pronounced effect when multiple modes are considered*.

Further observations concerning the approximate harmonic balance results will be made after a comparison with the time integration results is completed in the following section.

4. NUMERICAL INTEGRATION TECHNIQUE

The system of multi-mode equations for the beam, equations (7), (10) and (11), may be numerically integrated at various frequencies of excitation until steady oscillations develop. These results can then be used to plot frequency response curves as was done with the harmonic balance method.

Equation (11) contains discontinuous terms because of the signum function used in the friction model. These discontinuities present computational difficulties during numerical integration. In particular, when sticking occurs, the discontinuity in the friction law causes the friction force to switch directions excessively, at times, with every time step. This can lead to very high computational times, especially when using an automatic time-step control technique in the integration, which was the case in this research.

On the other hand, maintaining a constant time step through a sticking interval can lead to a significant loss of accuracy. To avoid these problems, a sticking condition was checked each time the slip velocity crossed zero. If the maximum available friction force was sufficient to prevent slipping, the time integration was restarted using a set of *linear* equations representing the beam's dynamics for complete sticking. After each time step, the sticking condition was then rechecked to determine if the beam was still sticking or

had started to slip. The theoretical development of the linear beam equations for the case of a stuck friction interface follows.

When complete sticking occurs at the damper, the expressions for kinetic and potential energy, as well as the expression for virtual work for the beam, equations (3), (4) and (5), remain unchanged. The damper constraint (7) is such that the damper displacement remains constant at the value at which sticking occurred, w_{d_0}. Application of component mode synthesis and Lagrange's equations now yields a completely linear system of equations:

$$m_i \ddot{z}_i + 2\zeta_i m_i \omega_i \dot{z}_i + m_i \omega_i^2 z_i = F(t)\phi_i(L) + \beta(t)\phi_i(D), \qquad \text{for } i = 1, NM, \tag{29}$$

$$\sum_{i=1}^{NM} z_i \phi_i(D) = w_{d_0}. \tag{30}$$

These equations can be reduced to eliminate $\beta(t)$ and the constraint condition (30) in the following manner. First, let the following represent "initial" modal quantities when sticking occurs:

$$\mathbf{z}_0 = \begin{bmatrix} z_{1_0} \\ z_{2_0} \\ \vdots \\ z_{NM_0} \end{bmatrix}, \qquad \dot{\mathbf{z}}_0 = \begin{bmatrix} \dot{z}_{1_0} \\ \dot{z}_{2_0} \\ \vdots \\ \dot{z}_{NM_0} \end{bmatrix}.$$

For the duration of the sticking interval the modal displacements and velocities can be written as

$$\mathbf{z} = \mathbf{z}_0 + \mathbf{\Delta z}, \qquad \dot{\mathbf{z}} = \dot{\mathbf{z}}_0 + \mathbf{\Delta}\dot{\mathbf{z}}, \tag{31}$$

where $\mathbf{\Delta z}$ and $\mathbf{\Delta}\dot{\mathbf{z}}$ represent the dynamic motion of the beam after the onset of sticking.

Substitution of equations (31) into equations (29) and (30) yields

$$m_i \Delta\ddot{z}_i + 2\zeta_i m_i\omega_i \Delta\dot{z}_i + m_i\omega_i^2 \Delta z_i = F(t)\phi_i(L) + \beta(t)\phi_i(D) - 2\zeta_i m_i\omega_i \dot{z}_{i_0} - m_i \omega_i^2 z_{i_0}, \quad \text{for } = i = 1, NM, \tag{32}$$

$$\sum_{i=1}^{NM} \Delta z_i \phi_i(D) = 0. \tag{33}$$

These equations can be combined into a reduced set of $NM - 1$ equations using the component mode synthesis procedure outlined in reference [18]. Using this procedure, first one introduces the linear transformation

$$\mathbf{\Delta z}(t) = [\mathbf{S}]\mathbf{q}(t), \tag{34}$$

where

$$\mathbf{q} = \begin{bmatrix} \Delta z_2 \\ \Delta z_3 \\ \vdots \\ \Delta z_{NM} \end{bmatrix}$$

and $[\mathbf{S}]$ is a matrix that enforces the constraint condition

$$\Delta z_1 = -[\phi_2(D)/\phi_1(D)]q_1 - [\phi_3(D)/\phi_1(D)]q_2 \cdots - [\phi_{NM}(D)/\phi_1(D)]q_{NM-1}$$

as its first row such that

$$[\mathbf{S}] = \begin{bmatrix} -\phi_2(\mathrm{D})/\phi_1(\mathrm{D}) & -\phi_3(\mathrm{D})/\phi_1(\mathrm{D}) & \cdots & -\phi_{\mathrm{NM}}(\mathrm{D})/\phi_1(\mathrm{D}) \\ 1 & 0 & \cdots & 0 \\ \vdots & \vdots & \ddots & \vdots \\ 0 & 0 & \cdots & 1 \end{bmatrix}.$$

The transformation (34) is substituted into equation (32), and the result is premultiplied by $[\mathbf{S}]^{\mathrm{T}}$. One can easily verify that the term $[\mathbf{S}]^{\mathrm{T}}\beta\boldsymbol{\phi}(D) = 0$, where

$$\boldsymbol{\phi}(D) = \begin{bmatrix} \phi_1(D) \\ \phi_2(D) \\ \vdots \\ \phi_{NM}(D) \end{bmatrix},$$

The final result is the desired set of linear differential equations that describe the beam system when the interface is stuck:

$$[\mathbf{M}]\ddot{\mathbf{q}} + [\mathbf{C}]\dot{\mathbf{q}} + [\mathbf{K}]\mathbf{q} =$$

$$[\mathbf{S}]^{\mathrm{T}}F(t)\boldsymbol{\phi}(L) - [\mathbf{S}]^{\mathrm{T}}\begin{bmatrix} m_1\omega_1^2 z_{1_0} \\ m_2\omega_2^2 z_{2_0} \\ \vdots \\ m_{NM}\omega_{NM}^2 z_{NM_0} \end{bmatrix} - [\mathbf{S}]^{\mathrm{T}}\begin{bmatrix} 2\zeta_1\omega_1 m_1 \dot{z}_{1_0} \\ 2\zeta_2\omega_2 m_2 \dot{z}_{2_0} \\ \vdots \\ 2\zeta_{NM}\omega_{NM} m_{NM} \dot{z}_{NM_0} \end{bmatrix}, \qquad (35)$$

where

$$[\mathbf{M}] = [\mathbf{S}]^{\mathrm{T}}\begin{bmatrix} m_1 & 0 & \cdots & 0 \\ 0 & m_2 & \cdots & 0 \\ \vdots & \vdots & \ddots & \vdots \\ 0 & 0 & \cdots & m_{NM} \end{bmatrix}[\mathbf{S}],$$

$$[\mathbf{C}] = [\mathbf{S}]^{\mathrm{T}}\begin{bmatrix} 2\zeta_1\omega_1 m_1 & 0 & \cdots & 0 \\ 0 & 2\zeta_2\omega_2 m_2 & \cdots & 0 \\ \vdots & \vdots & \ddots & \vdots \\ 0 & 0 & \cdots & 2\zeta_{NM}\omega_{NM} m_{NM} \end{bmatrix}[\mathbf{S}],$$

$$[\mathbf{K}] = [\mathbf{S}]^{\mathrm{T}}\begin{bmatrix} m_1\omega_1^2 & 0 & \cdots & 0 \\ 0 & m_2\omega_2^2 & \cdots & 0 \\ \vdots & \vdots & \ddots & \vdots \\ 0 & 0 & \cdots & m_{NM}\omega_{NM}^2 \end{bmatrix}[\mathbf{S}].$$

Time integration of equation (35) is continued until it is determined that the system is no longer stuck. This determination is made easily if one notes that $\beta(t)$ is the force of constraint. The value of $\beta(t)$ can be obtained from any of the NM equations (29); in this study the first modal equation in equation (29) is used. It can be shown that the interface will remain stuck provided that

$$\mu(N_0 + K \tan\gamma\,|w_d\,|) \geqslant |\beta(t) + (N_0 + K \tan\gamma\,|w_d\,|) \tan\gamma \operatorname{sgn}(w_d)|. \tag{36}$$

Once it has been determined that the system is no longer stuck, the numerical integration procedure is restarted using equations (7), (10), (11).

5. COMPARISON OF HARMONIC BALANCE AND NUMERICAL INTEGRATION RESULTS

The accuracy of the harmonic balance results with respect to time integration results is now examined. This is important in determining the extent to which conclusions based on the harmonic balance results can be trusted. Based on the preliminary results from harmonic balance, three assumed modes of vibration were deemed to be sufficient in the frequency range $0 < r < 8$, for $\gamma \leqslant 35^\circ$.

Figure 5 shows frequency response comparisons between harmonic balance and numerical integration at a ramp angle of 5° using a one mode and a three mode beam model. Qualitatively, the multi-mode results compare well with the results using only one mode. This is an important observation since it suggets that the results and conclusions obtained using a one-mode analysis in earlier research efforts [17] are generally supported by the multi-mode analysis in the low frequency range.

It is seen that the harmonic balance results as compared to numerical integration are very good over the frequency range, $r > 2{\cdot}7$. At lower frequencies of excitation where stick/slip motion is much more prevalent, however, there is quite a large discrepancy. This stick/slip motion is characterized by the dry friction damper "sticking" or "locking" for a short time each time the velocity reverses direction. The accuracy of the first order harmonic balance is degraded in the case of stick/slip motion because the intermittent sticking adds higher harmonic content to the response, which can excite higher modes of vibration [14]. In addition, the inaccuracy of the harmonic balance method in predicting the phase shift between input and output as noted in reference [17] also contributes to significant errors in displacement amplitude predictions at low forcing frequencies.

The effect of the addition of higher modes of vibration is clearly evident in the numerical integration results using three modes. Internal resonance peaks are observed in the regions around $r = 1$–$1{\cdot}2$; $1{\cdot}4$–$1{\cdot}6$, $1{\cdot}9$–$2{\cdot}1$; $2{\cdot}4$–$2{\cdot}7$ and $5{\cdot}8$–$6{\cdot}0$. These peaks are induced by

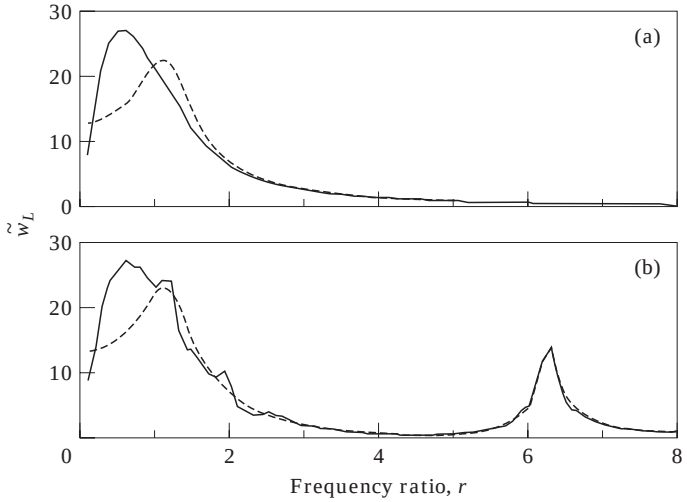

Figure 5. Frequency response curves for ramp angle = 5°. (a) $NM = 1$, (b) $NM = 3$. Key: - - - -, harmonic balance; ——, time integration.

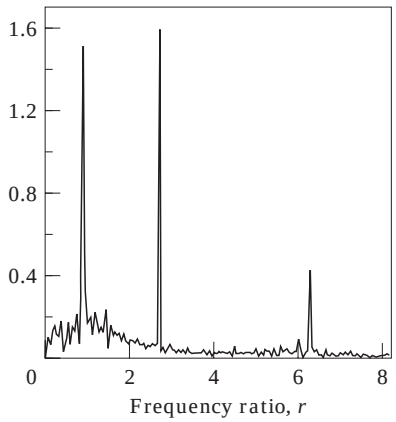

Figure 6. Fast Fourier transform; ramp angle = 5°; $NM = 3$; forcing frequency at $r = 2{\cdot}7$.

harmonics of the forcing function in those frequency ranges. As an example, the area of transition at $r = 2{\cdot}7$ is analyzed in detail. At forcing frequencies higher than this, there is good agreement between the harmonic balance and time integration predictions. Frequencies below 2·7 indicate the emergence of an internal resonance peak. A Fast Fourier Transform (FFT) of the steady state time response of the non-dimensional beam end displacement for $r = 2{\cdot}7$ is presented in Figure 6. It appears from this plot that the resonant peak is caused by a combination of the third subharmonic of the forcing exciting the first beam mode at $r = 0{\cdot}903$ and of the seventh multiple of the third subharmonic exciting the second beam mode at $r = 6{\cdot}32$. (Note that the assumed first and second natural frequencies of the undamped clamped–free beam are 152·3 rad/s $\{r = 1\}$ and 954·7 rad/s $\{r = 6{\cdot}27\}$.)

Figure 7 is a plot of the magnitudes of the modal amplitudes, z_1, z_2, and z_3, at varying excitation frequencies. This plot helps to confirm the above observation at $r = 2{\cdot}4$ to 2·7. Similar analysis of the peaks at $r = 1{\cdot}1$, 1·5, 1·9 and 5·9 indicate that they are the result of combinations of the third and fifth harmonics of the forcing frequency exciting combinations of the first, second and third beam modes.

To confirm the general qualitative agreement between the one mode and multi-mode solutions, Figure 8 is a plot of harmonic balance versus numerical integration results at

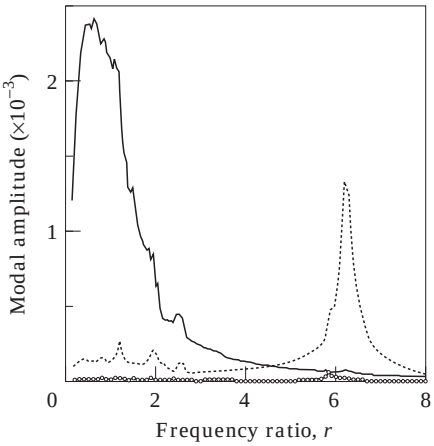

Figure 7. Modal amplitude contributions; ramp angle = 5°: ——, z_1; - - - -, z_2; -○-○-○-○-, z_3.

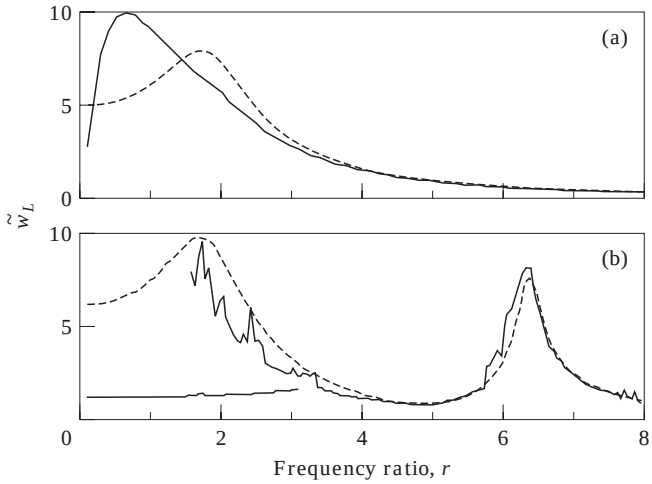

Figure 8. Frequency response curves for ramp angle = 14°; (a) $NM = 1$; (b) $NM = 3$. Key as in Figure 5.

a ramp angle of 14°. This is an especially interesting angle since it was shown in reference [17] that nearly maximum sticking occurs for the one mode approximation at this particular angle given the parameters in Table 1. It is interesting to note the increased occurrence of internal resonance peaks evident in the multi-mode solution. This is due to the more prevalent stick/slip behavior and the resulting increase in higher harmonic content of the response.

It is also most interesting to note the existence of multiple equilibrium solutions for the multi-mode results evident in Figure 8(b). This type of behavior was also observed in the single-degree-of-freedom system analyzed in reference [17] and it was found that both solution branches were stable. As such, both solution branches must be considered when analyzing the dynamic response of the system. If one were unaware of the existence of the upper solution branch, forced response amplitudes could be significantly underpredicted, leading to premature component failure. While operating along the lower amplitude solution branch, a sufficiently large disturbance could cause the system to jump to the higher amplitude branch. Therefore, the existence of these two stable solution branches could have a significant impact on design considerations.

6. DAMPING CONSIDERATIONS

A key finding in reference [17] was that the damping provided by displacement-dependent dry friction was similar to linear structural damping. As such, the equivalent damping ratio, ζ, was shown to be relatively insensitive to changes in the amplitude of the response for relatively large amplitudes.

To provide evidence of this observation for the multi-mode case, a bandwidth method or half-power method analysis was performed on the second resonant peak. Figure 9 is a plot of multi-mode frequency response curves of this resonant peak for a variety of forcing levels. To clarify the corresponding increase in the levels of the displacement response, the *dimensional* end beam displacement is plotted on the y-axis. Using the half-power method, it was found that the equivalent linear damping ratio for each curve was approximately equal to 0·017. Thus, regardless of the levels of displacement response, the equivalent damping ratio remained basically unchanged. Another key observation was

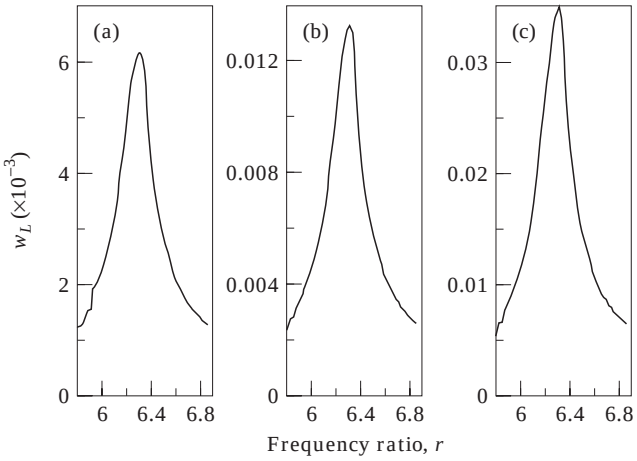

Figure 9. Frequency response curves for beam end displacement (m), second resonant peak; ramp angle = 5°; $NM = 3$, $N_0 = 5$ N, $\zeta_i = 0{\cdot}01$; various forcing amplitudes: (a) $F = 10$ N, (b) $F = 20$ N, (c) $F = 50$ N.

that the damping of this second mode was much less than that provided in the region of the fundamental mode when compared to the results of reference [17].

It was also noted in reference [17] that in the absence of the preload ($N_0 = 0$), the friction force exactly satisfies the requirements of linear structural damping. That is, it provides a force that is proportional to displacement but in phase with velocity. To further confirm this observation, the preload and applied viscous damping were removed and additional analyses were conducted. Figure 10 is a plot of these results. To construct this plot, several half power analyses were again conducted on the second resonant peak at various forcing levels. The calculated equivalent damping ratio was then plotted against the corresponding peak dimensional end displacement. Again, the invariance of the equivalent damping ratio to changes in displacement amplitude suggests that the damping properties of the second resonant peak bear a close resemblence to those normally associated with linear structural damping.

7. CONCLUSIONS

A multi-degree-of-freedom model of a beam-like structure damped with a displacement-dependent friction force has been studied. These results qualitatively agree with the results obtained analyzing the same structure using a SDOF model [17]. Both the single and multiple mode analyses suggest that it may be possible to enhance the vibration suppression properties of dry friction through the judicious selection of the ramp angle associated with the interface connection.

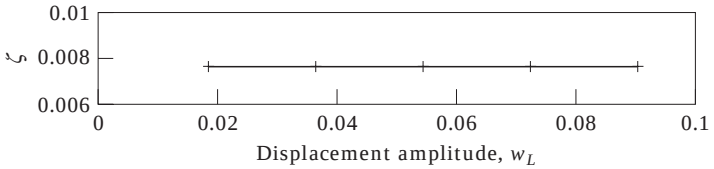

Figure 10. Equivalent damping ratio versus beam end displacement amplitude in m: second resonant peak; ramp angle = 5°; $NM = 3$, no viscous damping; no preload, $N_0 = 0$.

It is found that the ability to control the amplitude of the response is a function of the frequency range considered. In general, near modal resonance peaks, the amplitude of the response decreases with increasing ramp angles. However, in an "overlapping" region between resonance peaks, the amplitude of the response actually increases with increasing ramp angle.

Both harmonic balance and time integration techniques were used in the analysis of this system. It is shown that the presence of stick-slip motion and the inability of the harmonic balance technique to predict the proper phase between the input force and the response displacement at low frequencies of excitation result in significant errors in the harmonic balance solution. In addition, time integration of the multi-mode model reveals numerous internal resonance peaks. These peaks are the result of higher modes of vibration being excited by the higher harmonic frequency content in the stick/slip response.

An analysis of the damping characteristics indicated that the dry friction force is most effective in damping the fundamental mode. The other critical observation was that this damping contribution by the displacement-dependent dry friction damper is still linear structural-like in nature when multi-modes are considered and relatively insensitive to changes in the amplitude of the response. This result indicates that in the case of turbine or compressor blades, this type of damper arrangement may be effective in the suppression of flutter.

ACKNOWLEDGMENTS

This work was partially supported by ONR Grant # N00014-94-1-0517. Dr. Geoffrey L. Main is the contract monitor.

REFERENCES

1. R. L. Bielawa 1978 *American Society of Mechanical Engineers*, *Journal of Machine Design* **100**, 222–228. An analytic study of the energy dissipation of turbomachinery bladed-disk assemblies due to intershroud segment rubbing.
2. K. E. Beucke and J. M. Kelly 1985 *International Journal of Non-Linear Mechanics* **23**, 211–238. Equivalent linearizations for practical hysteretic systems.
3. C-H. Menq, J. H. Griffin and J. Bielak 1986 *American Society of Mechanical Engineers*, *Journal of Engineering for Gas Turbines and Power* **108**, 300–305. The influence of a variable normal load on the forced vibration of a frictionally damped structure.
4. C-H. Menq, J. H. Griffin and J. Bielak 1986 *American Society of Mechanical Engineers*, *Journal of Vibration*, *Acoustics*, *Stress and Reliability in Design* **108**, 50–55. The forced response of shrouded fan stages.
5. J. R. Anderson and A. A. Ferri 1990 *Journal of Sound and Vibration* **140**, 287–304. Behavior of a single-degree-of-freedom system with a generalized friction law.
6. A. A. Ferri and A. C. Bindemann 1992 *American Society of Mechanical Engineers*, *Journal of Vibration and Acoustics* **114**, 289–296. Damping and vibration of beams with various types of frictional support conditions.
7. B. Feeny and F. C. Moon 1994 *Journal of Sound and Vibration* **170**, 303–323. Chaos in a forced dry-friction oscillator: experiments and numerical modelling.
8. A. A. Ferri and B. S. Heck 1992 *American Institute of Aeronautics and Astronautics*, *Journal of Guidance*, *Control and Dynamics* **15**, 1258–1264. Analytical investigation of damping enhancement using active and passive structural joints.
9. F. Pfeiffer and M. Hajek 1992 *Philosophical Transactions of the Royal Society of London A* **338**, 503–517. Stick-slip motion of turbine blade dampers.
10. I. Tadjbakhsh and B. C. Lin 1987 *Earthquake Engineering and Structural Dynamics* **15**, 799–813. Displacement-proportional friction (DPF) in base isolation.
11. T. J. Hertz and E. F. Crawley 1984 *AIAA Dynamics Specialists Conference*, 17–18 *May*, *Palm Springs*, *California*. Damping in space structure joints.

12. N. Makris and M. C. Constantinou 1991 *Mechanics of Structures and Machines* **19**, 477–500. Analysis of motion resisted by friction. I. Constant Coulomb and linear/Coulomb friction.
13. A. Muszyńska and D. I. G. Jones 1983 *American Society of Mechanical Engineers*, *Journal of Vibration*, *Acoustics*, *Stress and Reliability in Design* **105**, 434–500. A parametric study of dynamic response of a discrete model of turbomachinery bladed disk.
14. A. A. Ferri and E. H. Dowell 1988 *Journal of Sound and Vibration* **124**, 207–224. Frequency domain solutions to multi-degree-of freedom, dry friction damped systems.
15. A. A. Ferri and E. H. Dowell 1985 *Journal of Sound and Vibration* **101**, 55–74. The behavior of a linear, damped modal system with a non-linear spring-mass dry friction damper system attached, Part II.
16. A. A. Ferri, 1995 *American Society of Mechanical Engineers*, *Journal of Vibration and Acoustics* **117(B)**, 196–206. Friction damping and isolation systems.
17. W. E. Whiteman and A. A. Ferri 1996 *Journal of Sound and Vibration* **198**, 313–329. Displacement-dependent dry friction damping of a beam-like structure.
18. R. R. Craig, Jr. 1981 *Structural Dynamics*: *An Introduction to Computer Methods*. New York: John Wiley.
19. C. Pierre, A. A. Ferri and E. H. Dowell 1985 *American Society of Mechanical Engineers*, *Journal of Applied Mechanics* **51**, 958–964. Multi-harmonic analysis of dry friction damped systems using an incremental harmonic balance method.
20. Y. Ren and C. F. Beard 1994 *Journal of Sound and Vibration* **172**, 593–604. A new receptance-base perturbative multi-harmonic balance method for the calculation of steady state response of non-linear systems.
21. J. H. Wang and W. K. Chen 1993 *American Society of Mechanical Engineers*, *Journal of Engineering for Gas Turbines and Power* **115**, 294–299. Investigation of the vibration of a blade with friction damper by HBM.
22. F. H. Ling and X. X. Wu 1987 *International Journal of Non-Linear Mechanics* **22**, 89–98. Fast Galerkin method and its application to determine the periodic solutions of non-linear oscillations.